Journal of Applied Physics

RESEARCH ARTICLE | DECEMBER 04 2025

Infrared phonons in monoclinic $Hf_{0.5}Zr_{0.5}O_2$ thin films

V. Železný ; E. de Prado ; E. Barriuso ; P. A. Algarabel ; J. A. Pardo ; S. Kamba

J. Appl. Phys. 138, 214101 (2025)
https://doi.org/10.1063/5.0297535

AIP Publishing

Journal of Applied Physics ARTICLE pubs.aip.org/aip/jap

Infrared phonons in monoclinic $Hf_{0.5}Zr_{0.5}O_2$ thin films

Cite as: J. Appl. Phys. **138**, 214101 (2025); doi: 10.1063/5.0297535
Submitted: 20 August 2025 · Accepted: 17 November 2025 ·
Published Online: 4 December 2025

V. Železný,[1,a)] E. de Prado,[1] E. Barriuso,[2] P. A. Algarabel,[2,3] J. A. Pardo,[2,4] and S. Kamba[1]

AFFILIATIONS

[1]Institute of Physics, Academy of Sciences of the Czech Republic, Na Slovance 2, 182 00 Prague 8, Czech Republic
[2]Instituto de Nanociencia y Materiales de Aragón, Consejo Superior de Investigaciones Científicas, Universidad de Zaragoza, 50018 Zaragoza, Spain
[3]Departamento de Física de la Materia Condensada, Universidad de Zaragoza, 50009 Zaragoza, Spain
[4]Departamento de Ciencia y Tecnologia de Materiales y Fluidos, Universidad de Zaragoza, 50018 Zaragoza, Spain

[a)]**Author to whom correspondence should be addressed:** zelezny@fzu.cz

ABSTRACT

Infrared (IR) reflectance spectra of monoclinic $Hf_{0.5}Zr_{0.5}O_2$ (HZO) films with thickness in the range of 10–90 nm deposited on different cuts of Al_2O_3 and yttria-stabilized zirconia (YSZ) substrates were measured in the frequency region 30–4000 cm^{-1}. Several phonons belonging to HZO were observed even for the 10 nm films. X-ray diffraction measurements were used to determine the crystal structure of the films and their orientation with respect to the substrates. The phonon spectra of HZO films grown on the anisotropic $(1\bar{1}02)$ *R*-cut Al_2O_3 substrates exhibit strong anisotropy. Comparing them with the spectra of the films on isotropic YSZ substrates, it allows us to assign the symmetry and polarization of the phonons in HZO films. Fitting the IR spectra by the classical Lorentz model, we obtain the phonon parameters, their response functions, and their contribution to static permittivity. We also measured the IR reflectance of HfO_2, ZrO_2 and HZO ceramics and compared their phonon parameters with those of the corresponding thin films.

I. INTRODUCTION

Hafnia-based materials (HfO_2, ZrO_2 and $Hf_xZr_{1-x}O_2$) are interesting from several points of view. They are used as gate dielectrics in complementary metal–oxide–semiconductor (CMOS) devices[1–3] due to their high permittivity, which allows them to substitute SiO_2. Their major advantages are full compatibility with silicon technology and ease of preparation in the form of thin films.[4–7] They are expected to accelerate further progress in chip electronics.[8–10] Another unexpected effect, which has been predicted and observed in undoped HfO_2 films, is ferromagnetism,[11–14] despite the fact that Hf^{4+} and O^{2-} ions are not-magnetic.

The discovery of ferroelectricity in HfO_2 thin films,[15] antiferroelectricity, and a field-driven ferroelectric phase transition in pure ZrO_2 as well as a stable ferroelectric phase in $Hf_xZr_{1-x}O_2$[16] has sparked intense research activity in this family of materials. Bulk monoclinic HfO_2-based materials are not intrinsically ferroelectric and must be modified to exhibit such behavior. The ferroelectric phase has a non-equilibrium orthorhombic structure that can be stabilized in thin films[15,17] when the tetragonal-to-monoclinic phase transformation is suppressed, either by the strain from the substrate or by surface tension in nanometer-sized grains. The ferroelectric properties of these thin films can be further improved in solid solutions of HfO_2 and ZrO_2. $Hf_xZr_{1-x}O_2$ films are intensively studied, and their ferroelectricity is stable for x in the range (0.3–0.7), with remanent polarization peaking at x = 0.5.[16] The orthorhombic ferroelectric phase has also been stabilized in HfO_2 single crystals by yttrium and lutetium doping.[18,19] The influence of many other dopants has been reported.[20]

HfO_2 and ZrO_2 are isomorphic, fully miscible[21,22] and exhibit the same sequence of structural phase transitions. Under bulk and thermodynamic equilibrium conditions, they crystallize in several different phases:[23,24] monoclinic $P2_1/c$ (C_{2h}^5), $Z_{prim} = 4$ at room temperature; transforming to a tetragonal structure $P4_2/nmc$ (D_{4h}^{15}), $Z_{prim} = 2$ at about 1170 °C for ZrO_2 and 1700 °C for HfO_2; and finally to cubic structure $Fm\bar{3}m$ (O_h^5), $Z_{prim} = 1$ at about 2370 °C for

ZrO_2 and 2600 °C for HfO_2.[21,22,25] The phase transition temperatures depend on many factors,[26] but all these phases are centrosymmetric and thus non-ferroelectric. In addition, four metastable orthorhombic phases—*Pcba*, *Pnma*, *Pca*2_1, and *Pmn*2_1 (the latter two being ferroelectric)—can be observed and stabilized by applying mechanical stress from a substrate in thin film and by doping.[27,28]

Infrared (IR) and Raman (R) spectroscopies are known to be nondestructive and highly effective tools for studying the lattice dynamics of both bulk materials and thin films. Based on the selection rules for IR and Raman phonon activity, these techniques provide important information on the crystalline structure, enabling to distinguish crystal phases, optical phonons, and their role in phase transitions. This has been demonstrated recently comparing experimental spectroscopic and X-ray diffraction (XRD) data with first-principles theoretical studies of HfO_2-based materials.[25,29–31] A similar analysis has also been performed[32] to explain the phase transitions that are not driven by soft phonons at the center of the Brillouin zone. However, complete phonon assignment and understanding of their role in phase transitions have not yet been fully achieved.

The Raman spectra of HfO_2-based materials[33–37] have previously been measured mainly in the room-temperature monoclinic phase. Nevertheless, even for this phase, the results are not quite satisfactorily and fully interpreted as a result of the relatively large number of phonons. There are many theoretical first-principles calculations providing phonon properties,[21,22] which have been followed by other research studies. However, there is still a lack of reliable experimental Raman spectra for comparison, except for very recently published data on crystals[29] and thin films.[30] Not all phonon modes predicted by group-theoretical analysis have been clearly resolved or correctly assigned, as some of them are quite weak, broad, and overlapping. The situation is even more complicated for IR spectroscopy, as sufficiently large single crystals are not available. Early IR spectra were mostly measured on powder samples,[38,39] and only a few very recent studies focus on thin films[25,31,40] and crystals.[29] IR absorption and Raman spectroscopy with a diamond anvil cell were used to study the pressure dependence of the phase transitions in polar orthorhombic HfO_2 doped by Y.[41]

In this work, we present an IR reflectance study on monoclinic $Hf_{0.5}Zr_{0.5}O_2$ HZO films (space group $P2_1/c$) of various thicknesses deposited on single-crystalline yttria-stabilized ZrO_2 (YSZ) and Al_2O_3 substrates. We also demonstrate that reflectance measurements can provide important information about phonons, even in very thin films. By fitting the experimental reflectance data, we are able to evaluate the complex dielectric functions and extract phonon parameters. This allows us to assess the influence of substrates—such as strain and anisotropy—on the phonon spectra of the films. To support this, we compare our IR data with XRD measurements. Additionally, we measured and analyzed the IR spectra of HfO_2, ZrO_2 and HZO ceramic pellets to compare them with the results obtained in HZO epitaxial films.

II. SYMMETRY PHONON ANALYSIS

The high-temperature cubic phase adopts the fluorite (CaF_2) $Fm\bar{3}m$ structure, where the oxygen atoms occupy interstitial sites within the face-centered cubic structure formed by the Hf/Zr atoms. A factor-group analysis at the Γ point of the Brillouin zone yields $\Gamma_{vib}^{cub} = F_{1u}(IR) + F_{2u}(silent)$, where the activity of each mode is indicated in parentheses, and one additional F_{1u} mode is acoustic. The tetragonal $P4_2/nmc$ structure is obtained by doubling the unit cell through alternate displacements of oxygen atom pairs along the z direction. The vibrational representation decomposes as $\Gamma_{vib}^{tetra} = A_{1g}(R) + A_{2u}(IR) + 3E_g(R) + 2E_u(IR) + B_{2u}(silent) + 2B_{1g}(R)$, with additional A_{2u} and E_u modes being acoustic. In the monoclinic $P2_1/c$ phase, the unit cell doubles again compared to the tetragonal phase, and the previously identical oxygen atoms in each pair become distinct. The factor-group analysis gives $\Gamma_{vib}^{mono} = 9A_g(R) + 9B_g(R) + 8A_u(IR) + 7B_u(IR)$, with additional $A_u + 2B_u$ modes as acoustic phonons. More examples of symmetry group analysis for ferroelectric and antiferroelectric phases can be found in the literature.[29,30]

III. EXPERIMENTAL

The HZO monoclinic films were fabricated using pulsed laser deposition (PLD) with a 248 nm KrF laser operating at 10 Hz repetition rate and with 1 J/cm^2 fluence, from a 99.99% pure ceramic target. During the deposition, single-crystal (001)-cut YSZ and Al_2O_3 substrates with various crystal orientations were maintained at 850 °C in a 100 mTorr pure oxygen atmosphere. The films had nominal thicknesses of 10, 12, 30, and 90 nm. They were colorless, shiny, and highly transparent. Their crystal characteristics have been already published in Ref. 42. For YSZ(001) substrates, the fourfold rotational symmetry along the [001] direction and a tilting of the c axis of the monoclinic thin film with respect to the substrate surface normal result in twin domains with four different orientations, projected of the (001) axis onto the substrate surface.[42]

XRD experiments on the Al_2O_3 substrates were performed using a SmartLab SE multipurpose diffractometer (Rigaku Corporation) with Cu K_α radiation and a HyPix-3000 2D detector. The incident beam optics included a parabolic Göbel mirror, and a 2.5° Soller slit and an incident slit and a mask of 0.5 and 2 mm, respectively. For the YSZ-supported epitaxial films, a Bruker D8 Advance diffractometer with monochromatic Cu-$K_{\alpha1}$ radiation, parallel-beam optics, and an Eulerian cradle was used for XRD analysis. The same device was used for the x-ray reflectivity measurements to determine the thickness of films. The details can be seen in part A of the supplementary material.

Ceramic powders for pellet preparation were sourced from Sigma-Aldrich [hafnium dioxide (IV)] and the American Elements (99.9% ZrO_2). These were pressed into pellets, heated below the monoclinic-to-tetragonal phase transition temperature, sintered, ground, and polished to optical quality.

The IR reflectance at near-normal incidence was measured over a broad frequency range (30–4000 cm^{-1}) using a Bruker IFS 113v Fourier-transform spectrometer equipped with DTGS pyroelectric detectors. KBr and broad-band far-IR Mylar beam splitters were used to cover the full spectral range. An aluminum mirror served as the reference. The spectra are presented only below 1000 cm^{-1} as no phonon modes were observed at higher frequencies. For HZO thin films on cubic YSZ, unpolarized radiation was used, while polarized radiation was employed for those grown on α-Al_2O_3 substrates. Attempts to measure phonon modes in polycrystalline HZO films on Si substrates were unsuccessful.

The normal-incidence reflectivity from a bulk surface is expressed as

$$R(\omega) = \left|\frac{\sqrt{\tilde{\varepsilon}(\omega)} - 1}{\sqrt{\tilde{\varepsilon}(\omega)} + 1}\right|^2. \quad (1)$$

The complex dielectric function $\tilde{\varepsilon}(\omega)$ for the bare substrates because of their broad reststrahlen bands is expressed by the generalized factorized (LO-TO) model,

$$\tilde{\varepsilon}(\omega) = \varepsilon_\infty \prod_{j=1}^{n} \frac{\omega_{\mathrm{LO}j}^2 - \omega^2 - i\gamma_{\mathrm{LO}j}\omega}{\omega_{\mathrm{TO}j}^2 - \omega^2 - i\gamma_{\mathrm{TO}j}\omega}, \quad (2)$$

where $\omega_{\mathrm{TO}j}$ and $\omega_{\mathrm{LO}j}$ are longitudinal and transverse frequencies of the jth vibrational mode, $\gamma_{\mathrm{LO}j}$ and $\gamma_{\mathrm{TO}j}$ are their damping factors, and ε_∞ represents the high-frequency dielectric constant due to electronic transitions. For the film and ceramics fits, the IR-active optical phonons, because their spectral features are much narrower, are modeled by the classical Lorentz formula consisting of the sum of n damped harmonic oscillators,

$$\tilde{\varepsilon}(\omega) = \varepsilon'(\omega) + i\varepsilon''(\omega) = \varepsilon_\infty + \sum_{j=1}^{n} \frac{\omega_{Pj}^2}{\omega_{\mathrm{TO}j}^2 - \omega^2 - i\omega\gamma_j}, \quad (3)$$

where ω_{Pj} is the phonon plasma frequency and the rest of parameters have the same meaning as in Eq. (2). The static permittivity, $\varepsilon(0)$, is given by the sum of the contributions of IR-active phonons and electronic contribution ε_∞,

$$\varepsilon(0) = \varepsilon_\infty + \varepsilon_{ph} = \varepsilon_\infty + \sum_{j=1}^{n} \Delta\varepsilon_j = \varepsilon_\infty + \sum_{j=1}^{n} \frac{\omega_{Pj}^2}{\omega_{\mathrm{TO}j}^2}, \quad (4)$$

where the mode strength $\Delta\varepsilon_j = \omega_{Pj}^2/\omega_{\mathrm{TO}j}^2$ is the contribution of the jth mode to $\varepsilon(0)$. In this way, IR spectroscopy can provide a low-frequency estimate of static dielectric permittivity.

If the film thickness is smaller than the IR radiation penetration depth, the substrate substantially influences the total reflectance spectrum.[43–45] It is taken into account by an "air–film–substrate" structure, which consists of the dielectric functions, ε_1=1 (air), $\varepsilon_2(\omega)$ (thin film), and $\varepsilon_3(\omega)$ (substrate). The total reflection coefficient at normal incidence for this structure with thickness d is

$$\tilde{r}_{123} = \frac{\tilde{r}_{12} + \tilde{r}_{23}\exp(i2\beta)}{1 - \tilde{r}_{12}\tilde{r}_{23}\exp(i2\beta)}, \quad (5)$$

where $\tilde{r}_{ij} = (\tilde{n}_i - \tilde{n}_j)/(\tilde{n}_i + \tilde{n}_j)$ are complex Fresnel coefficients, $\tilde{n}_i = n_i + ik_i = \sqrt{\tilde{\varepsilon}_i}$ are the refractive index and its real and imaginary parts, and $\beta = 2\pi\, d\omega\tilde{n}_2$ is a phase multiplier. The overall reflectance from the entire optical system, $R(\omega)$, is then given by

$$R(\omega) = |\tilde{r}_{123}|^2. \quad (6)$$

IV. RESULTS

A. Ceramic pellets

The reflectance spectra of HfO_2, ZrO_2 and HZO ceramic pellets were measured to compare their IR-active phonon parameters obtained by a fitting procedure with those of the HZO films. As the ceramic pellets consist of randomly oriented grains, a simple approximation is used for the total dielectric function, where it is volume-averaged over all the possible orientations of the grains as discussed in the Appendix of Ref. 46. In this case, all the IR-active phonons contribute to a reflectance spectrum irrespective of their polarization. As the reflectance was measured at room temperature, all the pellets are in the monoclinic phase (part B in the supplementary material), and 15 IR-active phonons predicted by group analysis ($\Gamma_{IR}^{mono} = 8A_u + 7B_u$) should be IR active. In the reflectance spectra, we could distinguish only 14 phonon frequencies for HfO_2, 13 for ZrO_2 and 8 for $Hf_{0.5}Zr_{0.5}O_2$. The reflectance spectra are shown in Fig. 1, and their phonon parameters are given in Table I. The results show a reasonable agreement with calculated and experimental data reported in the literature.[21,22,38,39] From Fig. 1, it is also clear that some of the reflectance peaks are not elementary, but their profile results from merging several peaks. This is the reason why not all of them are seen. The lower number of observed modes for the HZO pellet compared to the other two pellets is due to the reduced reflectance intensity and its rapid decrease with frequency, which are attributed to worse surface quality (i.e., porosity). When radiation encounters a rough or irregular surface, it generates diffuse reflection, which scatters radiation in different directions rather than just one as in the case of specular reflection. Some modes may be coalesced of the modes of elementary components (HfO_2 and ZrO_2) as is typical for mixed materials.

B. Substrates

In order to study thin films, we need to know the spectral properties of the substrates on which they are deposited. Sapphire (α-Al_2O_3) is a uniaxial crystal having a primitive rhombohedral

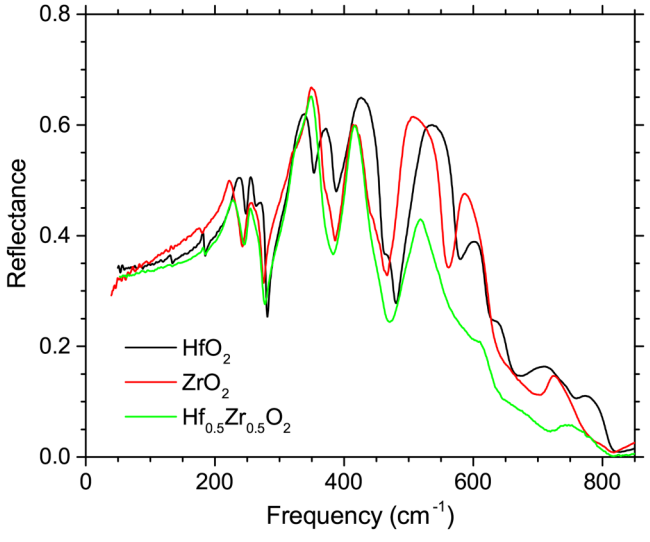

FIG. 1. Unpolarized room-temperature IR reflectance of HfO_2, ZrO_2 and HZO ceramic pellets.

TABLE I. IR-active phonon parameters (in cm^{-1}) of the HfO_2, ZrO_2 and HZO ceramic pellets obtained by fitting their reflectance spectra.

	HfO_2			ZrO_2			HZO		
j	ω_{TOj}	ω_{Pj}	γ_j	ω_{TOj}	ω_{Pj}	γ_j	ω_{TOj}	ω_{Pj}	γ_j
1	131	95	63	…	…	…	…	…	…
2	183	103	23	178	71	16	…	…	…
3	239	269	17	227	308	24	231	241	25
4	258	232	13	258	182	11	260	215	21
5	271	180	9	267	324	23	…	…	…
6	332	545	23	321	324	23	327	344	29
7	364	387	24	342	602	29	343	271	23
8	…	…	…	…	…	…	401	353	97
9	407	501	39	406	494	32	407	240	25
10	466	54	7	445	134	18	…	…	…
11	507	469	45	490	543	42	507	274	47
12	591	179	35	574	257	35	581	473	218
13	634	102	28	668	315	119	…	…	…
14	700	341	103	721	171	40	…	…	…
15	771	143	43	755	139	65	…	…	…

cell with two Al_2O_3 formulas (10 atoms) or a conventional hexagonal cell with six Al_2O_3 units (30 atoms) and belongs to the space group $R\bar{3}c$. The Al atoms occupy 12(c) sites with the C_2 symmetry and the O atoms sit in 18(e) sites with the C_3 symmetry. The decomposition of lattice vibrations in irreducible representations yields $\Gamma = 2A_{1g}(R) + 2A_{1u} + 3A_{2g} + 2A_{2u}(IR) + 5E_g(R) + 4E_u(IR)$ and A_{2u} and E_u acoustic modes.[47–50]

In the Al_2O_3 crystal, the A_{2u} phonons are oriented along the crystallographic c axis, and the doubly degenerate E_u phonons are polarized in the plane perpendicular to this axis. It is easy to obtain the A_{2u} and E_u dielectric functions from the $(11\bar{2}0)$ A- and $(\bar{1}010)$ M-cuts orienting the IR electric field parallel and perpendicular to the c-axis. The (0001) C-cut surface provides only the E_u component. Our fitting of the α-Al_2O_3 substrate reflectance using Eqs. (1) and (2) results in the identification of $2A_{1u}$ phonons at 398 and 583 cm^{-1} and $4E_u$ phonons (at 385, 439, 569, and 634 cm^{-1}), which are in very good agreement with ellipsometric[48] and reflectance[47,49,51] measurements.

When reflectance is measured from the R-cut $(1\bar{1}02)$ crystal surface of an Al_2O_3 crystal, two polarizations can be distinguished. The $[\bar{1}101]$ (c') direction given by the projection of the crystal c axis on the cut surface and the dielectric function is

$$\varepsilon_\theta = \frac{\varepsilon_{E_u}\varepsilon_{A_{2u}}}{\varepsilon_{E_u}\sin^2\theta + \varepsilon_{A_{2u}}\cos^2\theta}. \quad (7)$$

$\theta = 57.6°$, which is the angle between the c axis and the crystal surface. The other direction is perpendicular to the previous one, and only the E_u phonons are active in it.

To test our measurements, we substitute into Eq. (7) the values for ε_{E_u} and $\varepsilon_{A_{2u}}$ calculated using the phonon parameters mentioned above, which were obtained from the reflectance measurements on the A- and C-cuts. The good agreement between our experimental and calculated spectra is demonstrated in Fig. 2. The

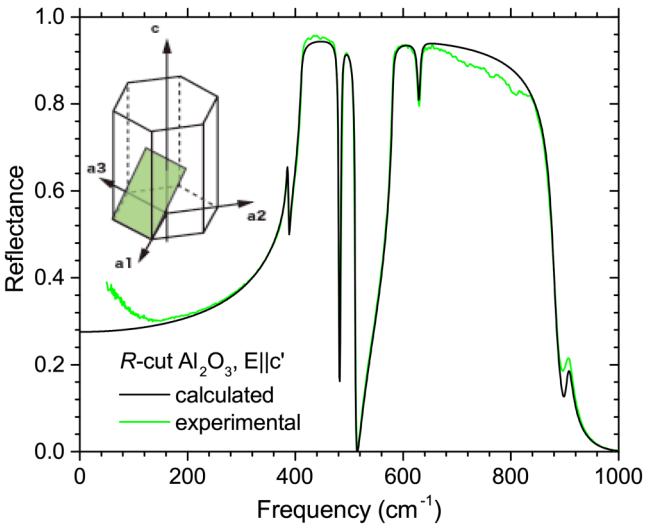

FIG. 2. Comparison of the Al_2O_3 substrate reflectivity calculated using Eq. (7) and the phonon parameters obtained from ellipsometry spectra,[48] and our experimental reflectance polarized along the projection of the c axis on the $(1\bar{1}02)$ crystal surface in the direction $[\bar{1}101]$. The inset shows the R-cut orientation.

small peak at 860 cm^{-1} results from the mixing of reflectance spectra with different longitudinal frequencies for polarizations along and perpendicular to the c axis using Eq. (7).

While the parameters of bulk α-Al_2O_3 phonons are well-known, the situation for YSZ is quite different. ZrO_2 itself is highly polymorphic, and its phases depend on temperature. When substituted by Y ions, its crystal lattice becomes additionally strongly dependent on their concentration.[52] Pure ZrO_2 at room temperature is monoclinic as discussed in Sec. II, and when fully stabilized by Y_2O_3 (in concentration higher than 12%), a cubic phase is obtained.[53–55] The broad IR reflectance of the YSZ substrate shown in Fig. 3 consists of strongly overlapped phonon reststrahlen bands forming practically one modulated band similar to that reported by Pecharroman *et al.*[54] on nearly 20% YSZ. No IR anisotropy was observed in our substrates spectra giving an evidence that the substrate is either in a cubic or polydomain phase. Fitting the substrate reflectance, five IR-active bands at 270, 327, 425, 621, and 743 cm^{-1} can be resolved. Comparing our phonon parameters with those reported in the literature[53–55] for varying Y doping, they show high similarity with those in a cubic phase. The cubic structure was also confirmed by XRD.[42]

C. Thin films

The room-temperature IR unpolarized reflectance spectra of monoclinic HZO films with 10, 30, and 90 nm thickness deposited on the (001) surface of a cubic YSZ substrate are shown in Fig. 3. As the films are substantially thinner than the substrates, the spectra are dominated by the strong restrahlen bands of the substrates. The spectral features of deposited films appear as a

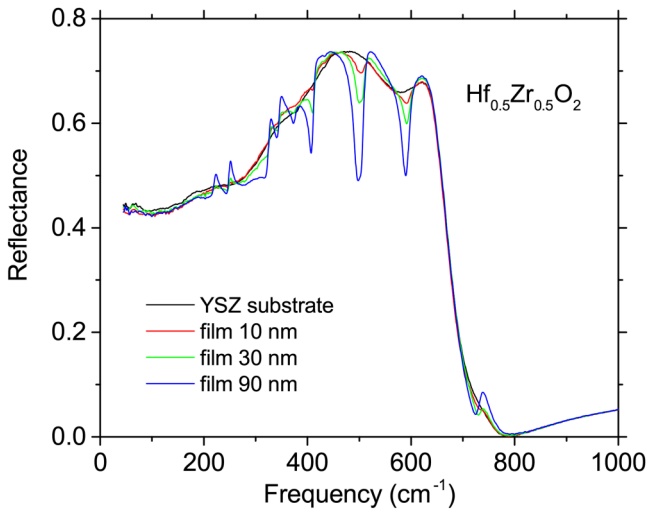

FIG. 3. Unpolarized IR reflectance of an yttria-stabilized zirconia (YSZ) substrate and PLD deposited HZO thin films of varying thicknesses on the YSZ substrates.

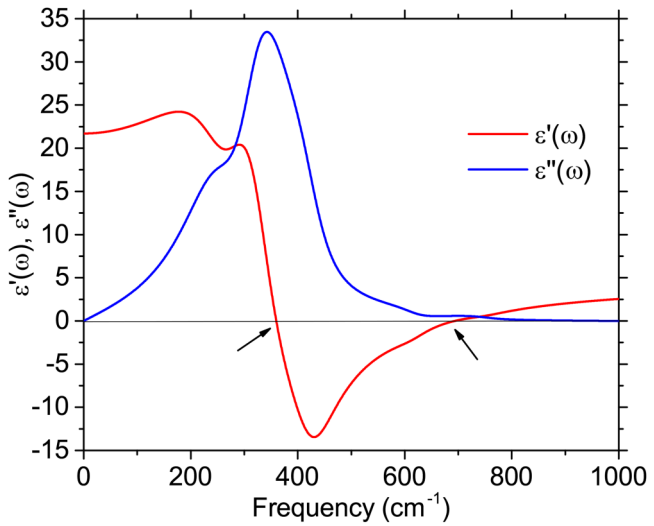

FIG. 4. Real and imaginary parts of YSZ used as a substrate for HZO films. The arrows indicate the limits of the YSZ substrate reststrahlen band.

modulation of the substrate reflectance. Figure 3 also demonstrates the enhancement of the intensity of the film spectral bands with increasing thickness. It is worth noting that whereas the phonon bands in the films located below a substrate reststrahlen band show up as upward aiming peaks, the modes located in the substrate reststrahlen band in Fig. 3 ranging from 350 to 700 cm^{-1} manifest as notches on the substrate reflectance. This effect is due to the change of sign of the real part of the substrate dielectric function, which is positive outside and negative inside the substrate reststrahlen band, as demonstrated in Fig. 4. Comparing the phonon parameters in the HZO films with those observed on the ceramic pellets,[38] the sharper character of our film spectra is seen. It is caused by the higher quality of the epitaxial thin films and their perfect surfaces, which results in lower phonon damping.

The high quality of our films allowed us to determine the absolute value of reflectance, extract the phonon parameters, and to calculate both components (ϵ', ϵ'') of the complex dielectric function of the films. First, we determine the parameters of the bare substrate fitting its reflectance using Eqs. (1) and (2) for a bulk sample. Then, we fix all the parameters of the substrate and fit the reflectance of the substrate covered with a thin film using Eqs. (3), (5), and (6) for a two-slab system. This procedure allows us to extract all oscillator parameters for the characterization of the film modes. The fit results are shown in Table II. The real and imaginary parts of the dielectric function of the 90 nm HZO film grown on YSZ are presented in Fig. 5. They show nine phonon modes located at 223, 251, 327, 346, 378, 412, 504, 592, and 728 cm^{-1}. The factor-group analysis predicts for the monoclinic phase 15 ($8A_u + 7B_u$) IR-active modes. The parameters of the phonons observed in our spectra are similar to those reported in other experimental papers on similar materials. They are shown in Table II, and their symmetry assignment is in agreement with Refs. 21 and 22. The contribution of all the identified film phonons and electrons to the static permittivity $\varepsilon(0)$ obtained using Eq. (4) is about 20, which is in good agreement with theoretical values for the monoclinic phase of HfO_2 and ZrO_2.[21,22,56] It is also worth remarking that the positions of the film phonons in Fig. 3 are independent of the film thickness. It means that the effect of the biaxial strain imparted into the films by the substrate is not observed. In other words, the phonon frequencies in these films show negligible dependence on strain, which, as will be described in the next paragraph, is not negligible.

The x-ray structural study of the same HZO thin films on YSZ substrates[42] has shown that they have a monoclinic structure. The reciprocal space maps (RSMs) around the 113 reflection and transmission electron microscopy observations show that the films are coherently strained and their in-plane lattice parameters match those of the substrate.[42] The strain imposed by the YSZ substrate on the film is tensile along the a axis (+0.3%) and compressive along the b axis (−0.8%), which gives rise to a distorted monoclinic structure of the film with lattice parameters ($a = b = 5.15$ Å). The epitaxial relation is $Hf_{0.5}Zr_{0.5}O_2(001)\|YZS(001)$. Given the fourfold rotational symmetry around the [001] substrate direction, the tilting of the film c axis takes four different orientations, as seen in the inset of Fig. 5, which results in four twin domains. Further details are described in Ref. 42. When the polarized normal IR reflectance of such films is measured, no anisotropy in the spectra is observed as the fourfold symmetry averages all directions of polarization. In our IR spectra, we can resolve 9 of them (without possibility resolving their polarization) instead of 15 as it has been mentioned above. As HZO is a solid solution, its reflectance is a combination of the contributions of its HfO_2 and ZrO_2 components, which complicates the interpretation of the spectra. The spectra of both components are very similar, and therefore, the

TABLE II. IR-active phonon parameters (in cm^{-1}) of the HZO thin films on YSZ and *R*-cut Al_2O_3 substrates obtained by fitting their reflectance spectra.

	HZO/YSZ			HZO/Al_2O_3			HZO/Al_2O_3		
	Unpol.			A_u, $E \parallel c'$			B_u, $E \perp c'$		
j	ω_{TOj}	ω_{Pj}	γ_j	ω_{TOj}	ω_{Pj}	γ_j	ω_{TOj}	ω_{Pj}	γ_j
1	223	290	8	…	…	…	220	342	17
2	251	347	8	248	591	20	…	…	…
3	327	534	9	…	…	…	327	873	20
4	346	563	11	343	588	17	…	…	…
5	378	408	18	…	…	…	384	281	4
6	412	614	11	…	…	…	…	…	…
7	504	609	17	509	397	14	…	…	…
8	592	324	16	…	…	…	…	…	…
9	728	275	13	…	…	…	733	493	33

observed spectral features result from the merged and overlapped contributions of their components.

The IR reflectance of a 30 nm HZO film grown on the $(1\bar{1}02)$ *R*-cut Al_2O_3 substrate and the corresponding bare substrate is shown in Fig. 6. As the substrate is IR-anisotropic, polarized IR radiation was used to distinguish between the $4E_u$ substrate phonons *perpendicular* to the projection (c') in the $[11\bar{2}0]$ direction and the mixture of $2A_{2u}$ and $4E_u$ phonons *parallel* to the projection of the substrate c' axis in the $[\bar{1}101]$ direction on the *R*-cut surface as discussed in Subsection IV B. The total reflectance of the film deposited on this substrate is again dominated by several strong substrate reststrahlen bands, which originate from the Al_2O_3 polar phonons. In addition, much weaker spectral features superimposed

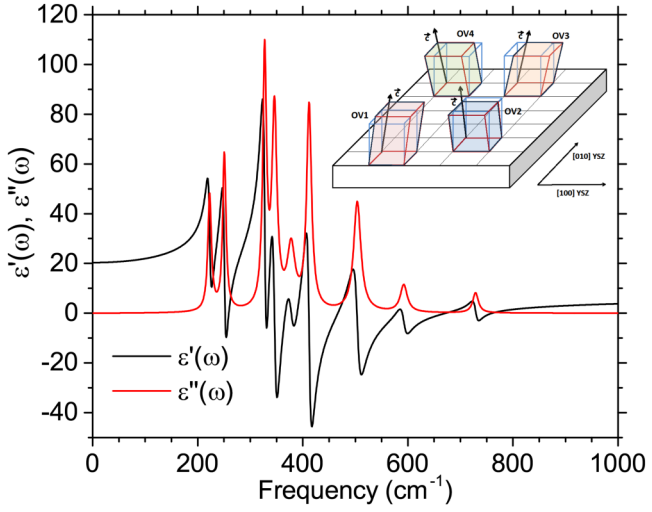

FIG. 5. Real and imaginary parts of the dielectric function for the 90 nm HZO thin film deposited on the YSZ substrate. The inset (modified from Ref. 42) shows the orientation of the film twin domains on the YSZ substrate.

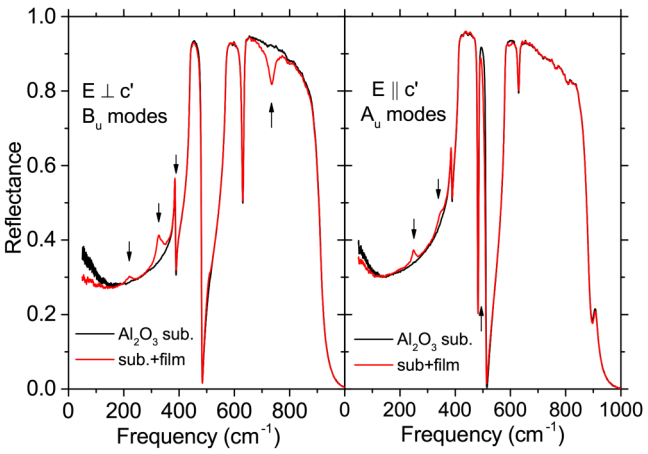

FIG. 6. Frequency dependent polarized reflectance of a bare *R*-cut Al_2O_3 substrate and the same substrate covered with a 30 nm $Hf_{0.5}Zr_{0.5}O_2$ thin film for the polarizations of electric field along and perpendicular to the c' direction. The symmetries of the thin film phonons are marked.

on the substrate structure come from the film phonons. Their frequencies are indicated in Fig. 6 by arrows. The film spectral features below 400 cm^{-1} point upward because the permittivity of the substrate is positive in this spectral range as discussed previously. The reflectance rise below ~100 cm^{-1} is caused by reflection from the rear substrate surface due to substrate transparency in this range. Phonons in the films existing at higher frequencies are difficult to resolve due to the complex and rich reflectivity spectrum of the substrate. Only the decrease in reflectance at 730 cm^{-1} caused by the strong phonon in the thin film is clearly visible in the left panel of Fig. 6.

The reflectance spectra were analyzed by the same fitting procedure, as it was employed for the HZO thin films on YSZ, using Eqs. (1) and (2) for the substrate and Eqs. (3), (5) and (6) for the film on the substrate. The phonon parameters were extracted and are shown in Table II. The real and imaginary parts of the film dielectric function are displayed in Fig. 7. In this case, only 4 phonons at 220, 327, 384, and 733 cm^{-1} for the polarization of the IR electric field $E \perp c'$ and 3 phonons at 248, 346, and 509 cm^{-1} for the polarization $E \parallel c'$ are resolved. The other phonons are hidden behind the rich structure of the substrate phonons. The difference in frequencies between the two polarizations indicates high anisotropy of the film, likely due to its clamping to the substrate. The longitudinal phonon frequencies are determined by plotting the loss function, $-Im(1/\tilde{\varepsilon})$, peaking for B_u phonons at 229, 376, 478, and 766 cm^{-1}, $E \perp c'$, and for A_u phonons at 288, 430, and 563 cm^{-1}, $E \parallel c'$ (part F in the supplementary material). The contribution of all the observed phonons and electrons to static permittivity, calculated using Eq. (4), is approximately 16, which is slightly lower than values reported in the literature.[21,22,56] This discrepancy is because not all the phonons contributing to $\varepsilon(0)$ are observed in our spectra, as they are overshadowed by much stronger substrate phonons.

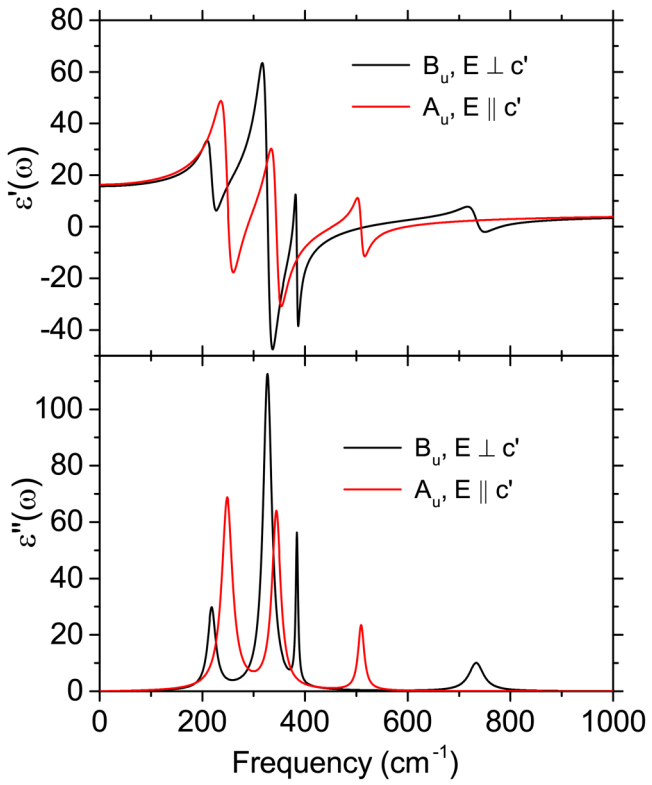

FIG. 7. Real and imaginary parts of a dielectric function of a 30 nm HZO film grown on the (1$\bar{1}$02) *R*-cut Al_2O_3 substrate calculated from the phonon parameters obtained by fitting the reflectance in Fig. 6. The anisotropy of the thin film is clearly seen.

We also measured the IR reflectance of 12 nm HZO thin films deposited on the (11$\bar{2}$0) *A*-, (0001) *C*-, and (1$\bar{1}$02) *R*-cuts of Al_2O_3 substrates. Surprisingly, no phonons were observed in the HZO films grown on the *A*- and *C*-Al_2O_3 cuts (part E in the supplementary material). On the contrary, the film phonons are seen on the films grown on the *R*-cut. The reflectance spectra are displayed in Fig. 8. The film spectral features for the 12 nm sample are similar to those of the 30 nm film, but their intensity is much weaker because of their smaller thickness.

A detailed display of the low-frequency (far-IR) part of the reflectance of the 12 nm HZO thin film on the *R*-cut of Al_2O_3 is presented in Fig. 9, where it is compared with the reflectance of the 30 nm one. For the IR electric field $E \perp c'$ direction, it shows 2 film phonons at 220 and 327 cm^{-1} for the 30 nm film and 2 phonons at 222 and 328 cm^{-1} for 12 nm thickness. For the $E \parallel c'$ polarization, there are 2 phonons at 248 and 346 cm^{-1} for the 30 nm film and 250 and 350 cm^{-1} for the 12 nm film. The width of the film-phonon features is relatively large in comparison with that of the substrate phonons, which complicates the precise determination of the phonon frequency and other parameters. This broadening is mainly due to the disorder induced by the mixing of HfO_2 and ZrO_2 components and the domain texture as has been

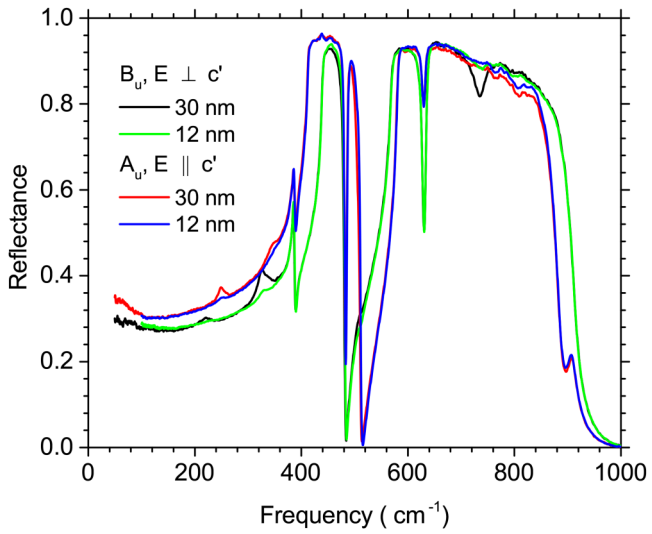

FIG. 8. Frequency dependent polarized reflectance of the 12 nm and 30 nm HZO thin films grown on the *R*-cut (1$\bar{1}$02) Al_2O_3 substrates for the polarization perpendicular to the *c*′ direction and the polarization along the *c*′ direction on the surface of the substrate.

observed by XRD. The phonon frequency shift between the 12 and 30 nm films is small (∼2–4 cm^{-1}) but is quite large (more than 20 cm^{-1}) between both polarized spectra. As the film phonon frequencies practically do not depend on the film thickness, it can be assumed that the influence of the strain coming from the

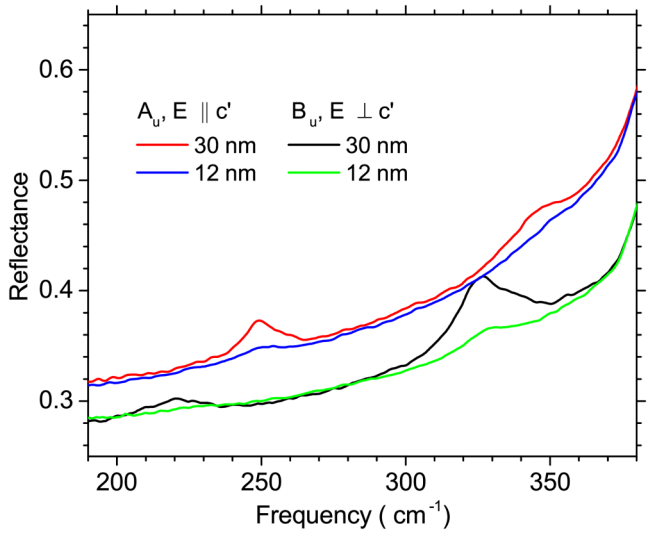

FIG. 9. The low-frequency part of polarized reflectance of the 12 and 30 nm HZO thin films grown on the *R*-cut (1$\bar{1}$02) Al_2O_3 substrate for the polarization perpendicular to the *c*′ axis and the polarization parallel to it.

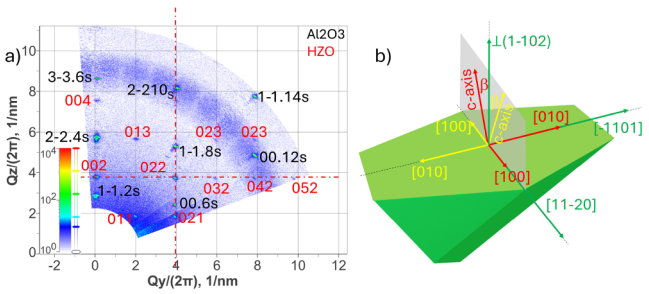

FIG. 10. (a) Wide-range RSM of the HZO (30 nm)/*R*-curAl_2O_3. Reciprocal space points are indexed according to their Miller indices: those of the layer are shown in red and those of the substrate in black. Dashed lines are visual guides. K_β reflections are non-labeled. (b) Schematic representation showing the epitaxial relationships between the film (red and yellow for D1 and D2 domain orientations) and the substrate (green).

film-substrate mismatch is small, and the film is either unrelaxed or only very slightly relaxed in the direction perpendicular to its surface.

The thin films on all the Al_2O_3 cuts were deposited under the same conditions; however, the phonon features are clearly identified only for the films on *R*-cuts. XRD measurements reveal that the films on *C*-cuts are basically non-symmetric and orthorhombic,[57] while those on *A*-cuts contain mixtures of monoclinic and orthorhombic phases (part C in the supplementary material). A reason for this difference may arise from the different arrangement of atoms on the surfaces of *A*, *C*, and *R* cuts. The *R*-plane of Al_2O_3 is known to have a distorted-square atomic distribution[58] that shows a good lattice match with the pseudocubic planes of ZrO_2 and HfO_2, having fluorite-related structures.

Indeed, epitaxial pure HfO_2 and ZrO_2 monoclinic thin films on Al_2O_3 *R*-cut substrates have been successfully deposited and characterized using XRD.[59,60] According to Ref. 60, the film-to-substrate out-of-plane orientation is given by $(001)HfO_2 \parallel (1\bar{1}02)\alpha\text{-}Al_2O_3$. There are two possible in-plane orientations: $[100]HfO_2 \parallel [110]\alpha\text{-}Al_2O_3$ and $[\bar{1}00]HfO_2 \parallel [110]\alpha\text{-}Al_2O_3$. The film lattice is compressed in the $[11\bar{2}0]$ and $[\bar{1}101]$ directions of Al_2O_3 in the surface plane and expanded in the perpendicular direction.

To clarify the results of the IR measurements, the orientation of the thin film was determined using wide-range RSMs. The low intensity resulting from the small thickness of the films made it impossible to perform measurements with a monochromator within a reasonable time. As a result, diffraction peaks corresponding to the characteristic Cu $K_{\alpha 2}$ and K_β lines are also observed in the maps. Figure 10(a) shows the RSM measured in an azimuth scan such that the *c* axis of the sapphire is contained within the map. All observed reflections were identified and attributed either to the monoclinic HZO thin film (marked in red) or to the Al_2O_3 substrate (marked in black), confirming the absence of mixed phases. The orientation of film on the *R*-cut Al_2O_3 substrate is similar to that found for pure HfO_2 and ZrO_2 films.[59,60] The pole finger for symmetric reflection indicates the presence of two crystalline domains (part D, labeled D1 and D2, in the supplementary material) rotated one another by 180° in the *R*-cut plane. Similar domains were observed in HfO_2 films.[60] The presence of the two domains does not affect the IR measurements,and they share the same twofold *b*-axis oriented along the substrate *c*′ direction.

TABLE III. IR-active phonon frequencies (in cm^{-1}). The columns (Col.) 1–3 show the phonon frequencies of HfO_2, ZrO_2 and HZO ceramic pellets obtained in this paper by fitting their reflectance spectra. Columns 10 and 11 show the phonon frequencies of the 30 nm HZO thin films on Al_2O_3 *R*-cut substrates polarized along the *c*′ direction (A_u phonons) and perpendicular to it (B_u phonons), and Col. 12 shows the phonon frequencies of the HZO thin film on the YSZ substrate. Our phonon frequencies are compared with those already published in Cols. 4–9.

Col. 1 HfO_2 ω_{TOj}	Col. 2 ZrO_2 ω_{TOj}	Col. 3 HZO ω_{TOj}	Col. 4 HfO_2 A_u[29]	Col. 5 HfO_2 B_u[29]	Col. 6 HfO_2 A_u[21]	Col. 7 HfO_2 B_u[21]	Col. 8 ZrO_2 A_u[22]	Col. 9 ZrO_2 B_u[22]	Col. l0 HZO/Al_2O_3 A_u, $E \parallel c'$	Col. 11 HZO/Al_2O_3 B_u, $E \perp c'$	Col. 12 HZO/YSZ Unpol.
131	…	…	134	…	140	…	…	…	…	…	…
183	178	…	185	…	190	…	181	…	…	…	…
…	227	…	…	…	…	…	…	224	…	220	223
239	…	231	…	240	…	246	242	…	248	…	251
258	258	260	256	255	255	262	253	…	…	…	…
271	267	…	…	…	…	…	…	305	…	…	…
332	321	327	…	330	…	354	…	319	…	327	327
364	342	343	362	345	393	378	347	355	346	…	346
407	406	401	415	403	…	…	401	414	…	384	378
466	445	407	…	…	445	449	478	483	…	…	412
507	490	507	508	518	529	553	…	…	509	…	504
591	574	581	607	…	…	…	571	…	…	…	592
634	668	…	661	…	661	…	634	…	…	…	…
700	721	…	…	…	683	…	…	711	…	…	…
771	755	…	…	741	…	779	…	…	…	733	728

Finally, a schematic representation of the orientation relationships between the film and the substrate is shown in Fig. 10(b).

The strong anisotropy observed in the IR reflectance and HZO film phonon parameters is induced by the strong anisotropy of the *R*-cut Al_2O_3 substrate surface. This arises from the rectangular atomic surface lattices for α-Al_2O_3 and HZO, which have similar cell parameters enabling lattice matchings. The third Al_2O_3 lattice parameter forms an angle ($\theta = 57.6°$) with respect to the surface and its projection (c' or the [$\bar{1}$101] direction) sets out the anisotropy direction. The film then grows in such a way that its monoclinic twofold axis b is oriented along the projection of the Al_2O_3 c' direction. It gives a possibility to distinguish between the phonons transforming according to A_u or B_u irreducible representations. The HZO A_u phonons are polarized along the twofold b axis, which is parallel to the Al_2O_3 c' direction, whereas the B_u phonons are polarized perpendicular to it. A complementary picture is provided by the films grown on the YSZ substrate where the tilting of the c axis has four-fold orientation. Both types of phonons (A_u and B_u) are observed simultaneously and form a doublet in the phonon spectrum. This is clearly observed in our experiments in Fig. 5. The polarized reflectance of the HZO films on the *R*-cut Al_2O_3 substrates allows us to distinguish A_u and B_u phonons and make their assignment (Table II). They agree with previously published theoretical and experimental data shown in Table III. This interpretation also suggests a possible explanation for the absence of observable IR-active phonons in the films grown on the *A*- and *C*- cuts. This could be a consequence of the good lattice match between the nearly square *R*-plane of Al_2O_3 and the HZO structure, which does not fulfill for the other substrate orientations.

V. CONCLUSIONS

We measured the IR reflectance of HZO thin films deposited on cubic YSZ and rhombohedral α-Al_2O_3 substrates to show that this technique is a useful tool for studying their phonons. We also applied this technique to the study of HfO_2, ZrO_2 and HZO ceramic pellets. Fitting the reflectance spectra, we determined their infrared dielectric functions and phonon parameters in the IR region. The XRD measurements were used to determine the crystal structure of the films and their orientation with respect to the substrates. Comparing the IR data with the XRD results, it was possible to assign the symmetries of the phonons and determine their polarization for the thin films deposited on *R*-cut Al_2O_3 substrates.

Al_2O_3 thin films as capping or blocking layers are recognized to improve the electrical properties of $Hf_xZr_{1-x}O_2$ solid solutions. Recently, it has been shown that inserting an ultrathin atomic Al_2O_3 layer improves the ferroelectricity and polarization stability of HZO films.[61] Our study, however, shows that the ferroelectricity of HZO thin films cannot be achieved if they are grown on the R-cut Al_2O_3 substrates, because the films are monoclinic.

SUPPLEMENTARY MATERIAL

See the supplementary material for additional supporting data on the crystal structure of thin films and pellets, and longitudinal phonon frequencies.

ACKNOWLEDGMENTS

This work has been supported by the Czech Science Foundation (Project No. 24-10791S) and by project TERAFIT-CZ.02.01.01/00/22_008/0004594 co-financed by the European Union and the Czech Ministry of Education, Youth and Sports. We also acknowledge financial support from Spanish Agencia Estatal de Investigación through projects PID2020-112914RB-I00 and PID2023-147211OB-C22 funded by MCIN/AEI/10.13039/501100011033 and from Gobierno de Aragón (Research Group E28_23R). E.B. acknowledges the support through the PRE2018-083233 predoctoral training grant. We thank Dr. Javier Blasco and Mr. Luis Torrejón at the Instituto de Nanociencia y Materiales de Aragón for providing us with some pellets used in this study.

AUTHOR DECLARATIONS

Conflict of Interest

The authors have no conflicts to disclose.

Author Contributions

V. Železný: Writing – original draft (equal); Writing – review & editing (equal). **E. de Prado:** Data curation (equal); Formal analysis (equal); Writing – original draft (equal). **E. Barriuso:** Data curation (equal). **P. A. Algarabel:** Data curation (equal). **J. A. Pardo:** Writing – review & editing (equal). **S. Kamba:** Writing – review & editing (equal).

DATA AVAILABILITY

The data that support the findings of this study are openly available in ASEP Repository at https://doi.org/10.57680/asep.0637780, Ref. 62.

REFERENCES

[1]A. I. Kingon, J. P. Maria, and S. K. Streiffer, "Alternative dielectrics for silicon-based transistor: Selection via multiple criteria," Nature **406**, 1032–1038 (2000).
[2]G. D. Wilk, R. M. Wallace, and J. M. Anthony, "High-κ gate dielectrics: Current status and materials properties considerations," J. Appl. Phys. **89**(10), 5243–5275 (2001).
[3]M. Jerman, Z. Qiao, and D. Mergel, "Refractive index of thin films of SiO_2, ZrO_2, and HfO_2 as a function of the films' mass density," Appl. Opt. **44**, 3006–3012 (2005).
[4]C. T. Hsu, Y. K. Su, and M. Yokoyama, "High dielectric constant of rf-sputtered HfO_2 thin films," Jpn. J. Appl. Phys. **31**(8R), 2501 (1992).
[5]J. Robertson, "High dielectric constant oxides," Eur. Phys. J. Appl. Phys. **28**(3), 265–291 (2004).
[6]J. Robertson, "High dielectric constant gate oxides for metal oxide Si transistors," Rep. Prog. Phys. **69**(2), 327–396 (2006).
[7]W. Banerjee, A. Kashir, and S. Kamba, "Hafnium oxide (HfO_2)—A multifunctional oxide: A review on the prospect and challenges of hafnium oxide in resistive switching and ferroelectric memories," Small **18**(23), 2107575 (2022).
[8]*High-K Gate Dielectrics: Why Do We Need Them?*, edited by M. Houssa (IOP Publishing, Bristol, UK, 2004).
[9]J. N. A. Matthews, "Semiconductor industry switches to hafnium-based transistors," Phys. Today **61**(2), 25 (2008).

[10]T. Mikolajick, U. Schroeder, and S. Slesazeck, "The past, the present, and the future of ferroelectric memories," IEEE Trans. Electron Devices **67**(4), 1434–1443 (2020).
[11]M. Venkatesan, C. B. Fitzgerald, and J. M. D. Coey, "Unexpected magnetism in a dielectric oxide," Nature **430**, 630 (2004).
[12]Q. Zhang, G. Chen, and S. Yunoki, "Surface ferromagnetism in HfO_2 induced by excess oxygen," Solid State Commun. **252**, 33–39 (2017).
[13]N. H. Hong, J. Sakai, N. T. Huong, N. Poirot, and A. Ruyter, "Role of defects in tuning ferromagnetism in diluted magnetic oxide thin films," Phys. Rev. B **72**, 045336 (2005).
[14]N. Hoa Hong, J. Sakai, N. Poirot, and V. Brizé, "Room-temperature ferromagnetism observed in undoped semiconducting and insulating oxide thin films," Phys. Rev. B **73**, 132404 (2006).
[15]T. S. Boscke, J. Muller, D. Bruhaus, U. Schroder, and U. Bottger, "Ferroelectricity in hafnium oxide thin films," Appl. Phys. Lett. **99**(10), 102903 (2011).
[16]J. Muller, T. S. Boscke, U. Schroder, S. Mueller, D. Brauhaus, U. Bottger, L. Frey, and T. Mikolajick, "Ferroelectricity in simple binary ZrO_2 and HfO_2," Nano Lett. **12**(8), 4318–4323 (2012).
[17]X. Sang, E. D. Grimley, T. Schenk, U. Schroeder, and J. M. LeBeau, "On the structural origins of ferroelectricity in HfO_2 thin films," Appl. Phys. Lett. **106**(16), 162905 (2015).
[18]X. Xu, F.-T. Huang, Y. Qi, S. Singh, K. M. Rabe, D. Obeysekera, J. Yang, M.-W. Chu, and S.-W. Cheong, "Kinetically stabilized ferroelectricity in bulk single-crystalline HfO_2:Y," Nat. Mater. **20**(6), 826–832 (2021).
[19]S. Wang, Y. Shen, X. Yang, P. Nan, Y. He, N. Lu, H. Yu, B. Ge, S. Zhang, and H. Zhang, "Unlocking the phase evolution of the hidden non-polar to ferroelectric transition in HfO_2-based bulk crystals," Nat. Commun. **16**(1), 3745 (2025).
[20]S. Starschich and U. Boettger, "An extensive study of the influence of dopants on the ferroelectric properties of HfO_2," J. Mater. Chem. C **5**(2), 333–338 (2017).
[21]X. Zhao and D. Vanderbilt, "First-principles study of structural, vibrational, and lattice dielectric properties of hafnium oxide," Phys. Rev. B **65**, 233106 (2002).
[22]X. Zhao and D. Vanderbilt, "Phonons and lattice dielectric properties of zirconia," Phys. Rev. B **65**, 075105 (2002).
[23]B. Johnson and J. L. Jones, "Structures, phase equilibria, and properties of HfO_2," in *Ferroelectricity in Doped Hafnium Oxide: Materials, Properties and Devices*, Woodhead Publishing Series in Electronic and Optical Materials, edited by U. Schroeder, C. S. Hwang, and H. Funakubo (Woodhead Publishing, 2019), Chap. 2, pp. 25–45.
[24]B. Cojocaru, D. Avram, R. Negrea, C. Ghica, V. G. Kessler, G. A. Seisenbaeva, V. I. Parvulescu, and C. Tiseanu, "Phase control in hafnia: New synthesis approach and convergence of average and local structure properties," ACS Omega **4**(5), 8881–8891 (2019).
[25]R. Cervasio, E. Amzallag, M. Verseils, P. Hemme, J.-B. Brubach, I. C. Infante, G. Segantini, P. Rojo Romeo, A. Coati, A. Vlad *et al.*, "Quantification of crystalline phases in $Hf_{0.5}Zr_{0.5}O_2$ thin films through complementary infrared spectroscopy and *ab initio* supercell simulations," ACS Appl. Mater. Interfaces **16**, 3829 (2024).
[26]J. Wang, H. P. Li, and R. Stevens, "Hafnia and hafnia-toughened ceramics," J. Mater. Sci. **27**, 5397–5430 (1992).
[27]T. D. Huan, V. Sharma, G. A. Rossetti, and R. Ramprasad, "Pathways towards ferroelectricity in hafnia," Phys. Rev. B **90**, 064111 (2014).
[28]V. Miikkulainen, M. Leskelä, M. Ritala, and R. L. Puurunen, "Crystallinity of inorganic films grown by atomic layer deposition: Overview and general trends," J. Appl. Phys. **113**(2), 021301 (2013).
[29]S. Fan, S. Singh, X. Xu, K. Park, Y. Qi, S. W. Cheong, D. Vanderbilt, K. M. Rabe, and J. L. Musfeldt, "Vibrational fingerprints of ferroelectric HfO_2," npj Quantum Mater. **7**(1), 32 (2022).
[30]U. Schroeder, R. Sachdeva, P. D. Lomenzo, B. Xu, M. Materano, T. Mikolajick, and A. Kersch, "Using Raman spectroscopy and x-ray diffraction for phase determination in ferroelectric mixed $Hf_{1-x}Zr_xO_2$-based layers," J. Appl. Phys. **132**(6), 214104 (2022).
[31]A. El Boutaybi, R. Cervasio, A. Degezelle, T. Maroutian, J.-B. Brubach, V. Demange, L. Largeau, M. Verseils, S. Matzen, G. Agnus *et al.*, "Ferroelectric ZrO_2 phases from infrared spectroscopy," J. Mater. Chem. C **11**(32), 10931–10941 (2023).
[32]S. Zhou, J. Zhang, and A. M. Rappe, "Strain-induced antipolar phase in hafnia stabilizes robust thin-film ferroelectricity," Sci. Adv. **8**(47), eadd5953 (2022).
[33]E. Anastassakis, B. Papanicolaou, and I. M. Asher, "Lattice dynamics and light scattering in hafnia and zirconia," J. Phys. Chem. Solids **36**(7-8), 667–676 (1975).
[34]G. A. Kourouklis and E. Liarokapis, "Pressure and temperature dependence of the Raman spectra of zirconia and hafnia," J. Am. Ceram. Soc. **74**(3), 520–523 (1991).
[35]C. Carlone, "Raman spectrum of zirconia-hafnia mixed crystals," Phys. Rev. B **45**, 2079–2084 (1992).
[36]S. N. Tkachev, M. H. Manghnani, A. Niilisk, J. Aarik, and H. Mändar, "Raman and Brillouin scattering spectroscopy studies of atomic layer-deposited ZrO_2 and HfO_2 thin films," Spectrochim. Acta A **61**(10), 2434–2438 (2005).
[37]J. L. Musfeldt, S. Singh, S. Fan, Y. Gu, X. Xu, S.-W. Cheong, Z. Liu, D. Vanderbilt, and K. M. Rabe, "Structural phase purification of bulk HfO_2:Y through pressure cycling," Proc. Natl. Acad. Sci. U.S.A. **121**(5), e2312571121 (2024).
[38]T. Hirata, "Infrared-reflectivity study of ZrO_2-HfO_2 solid solutions," Phys. Rev. B **50**, 2874–2879 (1994).
[39]H. Zhang, Y. Liu, K. Zhu, G. Siu, Y. Xiong, and C. Xiong, "Infrared spectra of nanometre granular zirconia," J. Condens. Matter Phys. **11**, 2035 (1999).
[40]S. T. Jaszewski, S. Calderon, B. Shrestha, S. S. Fields, A. Samanta, F. J. Vega, J. D. Minyard, J. A. Casamento, J.-P. Maria, N. J. Podraza *et al.*, "Infrared signatures for phase identification in hafnium oxide thin films," ACS Nano **17**(23), 23944–23954 (2023).
[41]J. L. Musfeldt, S. Singh, K. A. Smith, X. Xu, S.-W. Cheong, Z. Liu, D. Vanderbilt, and K. M. Rabe, "Pressure-driven polar orthorhombic to tetragonal phase transition in hafnia at room temperature," Chem. Mater. **37**(5), 1820–1825 (2025).
[42]L. Torrejón, E. Langenberg, C. Magén, A. Larrea, J. Blasco, J. Santiso, P. A. Algarabel, and J. A. Pardo, "Growth and structural characterization of strained epitaxial $Hf_{0.5}Zr_{0.5}O_2$ thin films," Phys. Rev. Mater. **2**, 013401 (2018).
[43]O. S. Heavens, *Optical Properties on Thin Solid Films* (Butterworths Scientific Publications, 1955).
[44]W. Vriens and W. Rippens, "Optical constants of absorbing thin films on a substrate," Appl. Opt. **22**(24), 4105–4110 (1983).
[45]V. Železný, I. Fedorov, and J. Petzelt, "FIR spectroscopic studies of ferroelectric films," Czech. J. Phys. **48**(5), 537–545 (1998).
[46]V. Železný, E. Cockayne, J. Petzelt, M. F. Limonov, D. E. Usvyat, V. V. Lemanov, and A. A. Volkov, "Temperature dependence of infrared-active phonons in $CaTiO_3$: A combined spectroscopic and first-principles study," Phys. Rev. B **66**(22), 224303 (2002).
[47]M. E. Thomas, S. K. Andersson, R. M. Sova, and R. I. Joseph, "Frequency and temperature dependence of the refractive index of sapphire," Infrared Phys. Technol. **39**(4), 235–249 (1998).
[48]M. Schubert, T. E. Tiwald, and C. M. Herzinger, "Infrared dielectric anisotropy and phonon modes of sapphire," Phys. Rev. B **61**, 8187–8201 (2000).
[49]G. Yu, N. L. Rowell, and D. J. Lockwood, "Anisotropic infrared optical properties of GaN and sapphire," J. Vac. Sci. Technol. A **22**(4), 1110–1114 (2004).
[50]Y. Kumagai, H. Yokoi, H. Tampo, Y. Tabata, and N. Kuroda, "Infrared study of sapphire α-Al_2O_3 by small-angle oblique-incidence reflectometry," J. Phys. Soc. Jpn. **81**(2), 024709 (2012).
[51]A. S. Barker, Jr., "Infrared lattice vibrations and dielectric dispersion in corundum," Phys. Rev. **132**(4), 1474 (1963).

[52]J. P. Goff, W. Hayes, S. Hull, M. T. Hutchings, and K. N. Clausen, "Defect structure of yttria-stabilized zirconia and its influence on the ionic conductivity at elevated temperatures," Phys. Rev. B **59**(22), 14202 (1999).
[53]D. W. Liu, C. H. Perry, and R. P. Ingel, "Infrared spectra in nonstoichiometric yttria-stabilized zirconia mixed crystals at elevated temperatures," J. Appl. Phys. **64**(3), 1413–1417 (1988).
[54]C. Pecharroman, M. Ocana, and C. J. Serna, "Optical constants of tetragonal and cubic zirconias in the infrared," J. Appl. Phys. **80**(6), 3479–3483 (1996).
[55]J. A. Nychka, M. R. Winter, D. R. Clarke, T. Naganuma, and Y. Kagawa, "Temperature-dependent optical reflectivity of tetragonal-prime yttria-stabilized zirconia," J. Am. Ceram. Soc. **89**(3), 908–913 (2006).
[56]D. Ceresoli and D. Vanderbilt, "Structural and dielectric properties of amorphous ZrO_2 and HfO_2," Phys. Rev. B **74**(12), 125108 (2006).
[57]E. Barriuso, P. Koutsogiannis, D. Serrate, J. Herrero-Martín H.-M., R. Jiménez, C. Magén, M. Algueró, P. A. Algarabel, and J. A. Pardo, "Direct epitaxial growth of polar $Hf_{0.5}Zr_{0.5}O_2$ films on corundum," Nanomaterials **12**(7), 1232 (2022).
[58]T. P. Trainor, P. J. Eng, G. E. Brown, Jr., I. K. Robinson, and M. De Santis, "Crystal truncation rod diffraction study of the α-Al_2O_3 (1 −1 0 2) surface," Surf. Sci. **496**(3), 238–250 (2002).
[59]H. Asaoka, Y. Katano, and K. Noda, "Epitaxial growth of zirconium dioxide films on sapphire substrates," Appl. Surf. Sci. **113-114**, 198–201 (1997).
[60]H. Mändar, R. Rammula, A. Aidla, and J. Aarik, "Atomic layer deposition of epitaxial HfO_2 thin films on *r*-cut sapphire," J. Mater. Res. **28**(13), 1680–1686 (2013).
[61]H. Chen, L. Tang, L. Liu, Y. Chen, H. Luo, X. Yuan, and D. Zhang, "Significant improvement of ferroelectricity and reliability in $Hf_{0.5}Zr_{0.5}O_2$ films by inserting an ultrathin Al_2O_3 buffer layer," Appl. Surf. Sci. **542**, 148737 (2021).
[62]V. Železný, E. Prado, E. Barriuso, P. A. Algarabel, J. A. Pardo, and S. Kamba, "HZO dataset," FZÚ DATA Scientific data - ASEP Repository (Library of the Academy of Sciences of the Czech Republic, 2025); https://doi.org/10.57680/asep.0637780.